Hindawi
Wireless Communications and Mobile Computing
Volume 2022, Article ID 8651956, 9 pages
https://doi.org/10.1155/2022/8651956

Research Article

Research on Printing Defects Inspection of Solder Paste Images

Min Qi,[1,2] **Ting Yin**,[1] **Gong Cheng**,[1] **Yuelei Xu**,[3] **Hongying Meng**,[4] **Yi Wang**,[1] **and Shanshan Cui**[1]

[1]*School of Electronics and Information, Northwestern Polytechnical University, Xi'an, China*
[2]*National Engineering Laboratory for Integrated Aero-Space-Ground-Ocean Big Data Application Technology, Xian, China*
[3]*Unmanned System Research Institute, Northwestern Polytechnical University, Xi'an, China*
[4]*Department of Electronic and Computer Engineering, Brunel University London, Uxbridge, UK*

Correspondence should be addressed to Min Qi; drqimin@nwpu.edu.cn

Received 31 December 2021; Accepted 28 January 2022; Published 25 March 2022

Academic Editor: Kalidoss Rajakani

Solder paste printing is the first part of the surface mount process flow; its postprinting defect inspection is particularly important. In this paper, we focus on studying the printing defects inspection algorithm for solder paste on PCB (Printed Circuit Board) images. The work proposes a number of methods to enhance the defects inspection performance of solder paste printing: a regional multidirectional data fusion image interpolation method, which can achieve fast and high precision image interpolation; a method for detecting solder paste areas with better accuracy, efficiency, and robustness; an improved connected domain labeling method to reduce time complexity; and defects detection and types classification method, which extracts features and centroid of every solder paste region and completes the inspection by comparing with a standard image. The experiments show that the defects inspection algorithm can detect the most common types of defects with low time consumption, high inspection accuracy, and classification accuracy.

1. Introduction

Figure 1(a) is an image of a PCB printed with solder paste and taken by a camera. Figure 1(b) is the corresponding standard image obtained by parsing the standard Gerber file of the PCB. As the image taken by the camera and the standard image do not match exactly in size and position, the registration operations for them need to be performed. One of the important steps in registration is image interpolation. After the registration is completed, the camera-taken image needs to be binarized to obtain a binary image with the solder paste area in white and the rest in black. In order to compare each solder paste region, a pass-through tagging operation is performed to assign a unique tag to each solder paste region in the binary image. Once the connected field is marked, the corresponding comparison inspection can be performed.

Existing image registration methods are divided into two main categories: feature-based registration and grayscale-based registration [1]. Firstly, we extract the features of the image, find out the transformation model and parameters, and finally transform the image as a whole [2–4]. The latter is based on the similarity of pixel grayscale to complete the matching, without extracting other feature information, but when the image is rotated and scaled, it has a huge impact on the algorithm [5]. Image interpolation is an important step in the image registration process. Existing image interpolation methods are broadly classified as adaptive and nonadaptive. Nonadaptive algorithms apply a fixed pattern to each pixel, mainly nearest neighbor, bilinear, and bicubic image interpolation; adaptive techniques require consideration of image edge information, texture, and pixel intensity [6, 7].

Image detection methods have their specific targets, and the corresponding detection methods are designed according to the application and image characteristics. For grayscale images, existing image detection methods are mainly based on two aspects: grayscale value discontinuity or grayscale value similarity. The former mainly relies on image edge detection and edge connectivity for implementation, such as improved Canny algorithm [8, 9], improved Prewitt operator [10], and Soble algorithm [11]. The latter, on the other hand, categorizes the image pixels according to a certain predefined rule, and typical

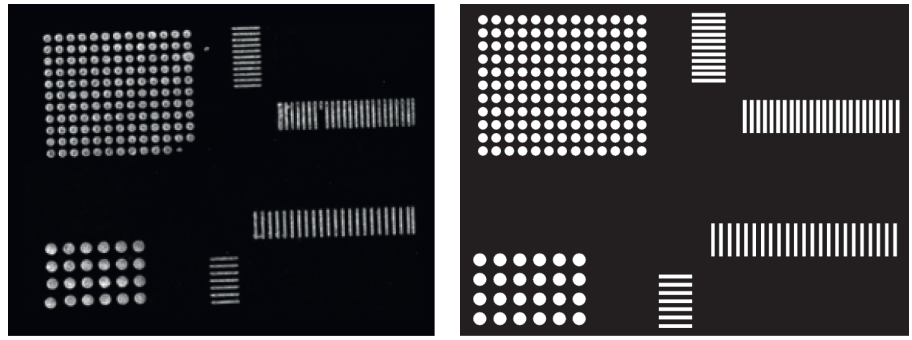

(a) (b)

Figure 1: PCB images. (a) The image taken using a camera. (b) The standard image.

algorithms include region generation and erosion algorithms and binarization algorithms.

Existing defect classification and inspection algorithms can be broadly classified into two categories: reference comparison method and reference-free verification method. The former is to compare the board to be tested with the standard board for pixel comparison and determine the defects by the difference between the two images. This type of method can inspect more types of defects but requires a high standard image and the registration accuracy of the two images. The latter does not require a standard image but generally requires the extraction of a large amount of feature information and has a high algorithm complexity. Depending on the type of inspected defects, researchers have proposed different inspection schemes [12, 13].

In this paper, the four aspects of image interpolation, solder paste area detection, connected domain labeling, and printing defect inspection are improved. The solution of this problem can enrich the connotation of machine vision in solder paste image and printing defect inspection and solve the urgent problem of SMT (Surface Mount Technology) production.

2. Methodology

2.1. Multidirection Data Fusion Image Interpolation Based on Regional Features. In order to meet the strict requirements of high-level industrial inspection in terms of accuracy and operation time, an image interpolation method with adaptive fusion calculation characteristics is proposed by referring to the idea of data fusion techniques, which is applied to edge regions in the images.

Let the corresponding point of the point to be interpolated in the source image be point P with coordinates (u, v), i and j are the largest integers not larger than u and v, respectively, and the grayscale values of the four pixel points in the 2×2 neighborhood of this corresponding point are $f(i, j)$, $f(i+1, j)$, $f(i, j+1)$, and $f(i+1, j+1)$, respectively.

The mean grayscale value E is

$$E = \frac{f(i, j) + f(i+1, j) + f(i, j+1) + f(i+1, j+1)}{4}. \quad (1)$$

The grayscale variance Var is

$$\mathrm{Var} = \frac{(E - f(i, j))^2 + (E - f(i+1, j))^2 + (E - f(i, j+1))^2 + (E - f(i+1, j+1))^2}{4} \quad (2)$$

According to the image characteristics, set the threshold T. If $\mathrm{Var} < T$, it is judged as a region of low grayscale variation, and the bilinear interpolation algorithm is used to interpolate the value. Otherwise, it is judged as an edge region with large grayscale variations, and interpolation is performed according to the following idea.

First, the estimated values of point P in the four interpolation directions of 45°, 135°, horizontal, and vertical are calculated and denoted as y_1, y_2, y_3, and y_4, respectively. The equations are as follows, where $S_{x,y}$ is the distance of point P from the source image Euclidean distance in pixels from the pixel with coordinates (x, y) in the image, where $x = i, i-1, i+1, i+2$; $y = j, j-1, j+1, j+2$.

$$y_1 = \frac{1}{2}\left(\frac{f(i+2, j-1)S_{i,j+1}^2 + f(i, j+1)S_{i+2,j-1}^2}{S_{i,j+1}^2 + S_{i+2,j-1}^2} + \frac{f(i+1, j)S_{i-1,j+2}^2 + f(i-1, j+2)S_{i+1,j}^2}{S_{i-1,j+2}^2 + S_{i+1,j}^2}\right),$$

$$y_2 = \frac{1}{2}\left(\begin{array}{l}\dfrac{f(i-1,j-1)S_{i+1,j+1}^2 + f(i+1,j+1)S_{i-1,j-1}^2}{S_{i+1,j+1}^2 + S_{i-1,j-1}^2} \\ \\ +\dfrac{f(i,j)S_{i+2,j+2}^2 + f(i+2,j+2)S_{i,j}^2}{S_{i+2,j+2}^2 + S_{i,j}^2}\end{array}\right),$$

$$y_3 = \begin{cases}\dfrac{1}{2}\left(\dfrac{f(i-1,j)S_{i+1,j}^2 + f(i+1,j)S_{i-1,j}^2}{S_{i+1,j}^2 + S_{i-1,j}^2} + \dfrac{f(i,j)S_{i+2,j}^2 + f(i+2,j)S_{i,j}^2}{S_{i+2,j}^2 + S_{i,j}^2}\right), & v - j <= 0.5, \\ \dfrac{1}{2}\left(\dfrac{f(i-1,j+1)S_{i+1,j+1}^2 + f(i+1,j+1)S_{i-1,j+1}^2}{S_{i+1,j+1}^2 + S_{i-1,j+1}^2} + \dfrac{f(i,j+1)S_{i+2,j+1}^2 + f(i+2,j+1)S_{i,j+1}^2}{S_{i+2,j+1}^2 + S_{i,j+1}^2}\right), & v - j > 0.5, \end{cases} \tag{3}$$

$$y_4 = \begin{cases}\dfrac{1}{2}\left(\dfrac{f(i,j-1)S_{i,j+1}^2 + f(i,j+1)S_{i,j-1}^2}{S_{i,j+1}^2 + S_{i,j-1}^2} + \dfrac{f(i,j)S_{i,j+2}^2 + f(i,j+2)S_{i,j}^2}{S_{i,j+2}^2 + S_{i,j}^2}\right), & u - i <= 0.5, \\ \dfrac{1}{2}\left(\dfrac{f(i+1,j-1)S_{i+1,j+1}^2 + f(i+1,j+1)S_{i+1,j-1}^2}{S_{i+1,j+1}^2 + S_{i+1,j-1}^2} + \dfrac{f(i+1,j)S_{i+1,j+2}^2 + f(i+1,j+2)S_{i+1,j}^2}{S_{i+1,j+2}^2 + S_{i+1,j}^2}\right), & u - i > 0.5. \end{cases}$$

Next, the distances from the point P to the four interpolation directions, denoted as r_1, r_2, r_3, and r_4, are calculated as follows:

$$r_1 = \frac{u - i + v - j - 1}{\sqrt{2}},$$

$$r_2 = \frac{u - i - v + j}{\sqrt{2}},$$

$$r_3 = \begin{cases} v - j, & j - v <= 0.5, \\ j - v + 1, & j - v > 0.5, \end{cases} \tag{4}$$

$$r_4 = \begin{cases} u - i, & u - i <= 0.5, \\ i + 1 - u, & u - i > 0.5. \end{cases}$$

The normalized formula for r_1, r_2, r_3, and r_4 is as follows:

$$d_k = \frac{r_k}{r_1 + r_2 + r_3 + r_4}, \quad k = 1, 2, 3, 4. \tag{5}$$

Then, the mean values of the grayscale gradient in the four interpolation directions are calculated, which are noted as g_1, g_2, g_3, and g_4, respectively, with the following equations:

$$g_1 = \frac{|f(i+2,j-1) - f(i+1,j)| + |f(i+1,j) - f(i,j+1)| + |f(i,j+1) - f(i-1,j+2)|}{3},$$

$$g_2 = \frac{|f(i-1,j-1) - f(i,j)| + |f(i,j) - f(i+1,j+1)| + |f(i+1,j+1) - f(i+2,j+2)|}{3},$$

$$g_3 = \begin{cases} \dfrac{|f(i-1,j) - f(i,j)| + |f(i,j) - f(i+1,j)| + |f(i+1,j) - f(i+2,j)|}{3}, & v - j <= 0.5, \\ \dfrac{|f(i-1,j+1) - f(i,j+1)| + |f(i,j+1) - f(i+1,j+1)| + |f(i+1,j+1) - f(i+2,j+1)|}{3}, & v - j > 0.5, \end{cases} \tag{6}$$

$$g_4 = \begin{cases} \dfrac{|f(i,j-1) - f(i,j)| + |f(i,j) - f(i,j+1)| + |f(i,j+1) - f(i,j+2)|}{3}, & u - i <= 0.5, \\ \dfrac{|f(i+1,j-1) - f(i+1,j)| + |f(i+1,j) - f(i+1,j+1)| + |f(i+1,j+1) - f(i+1,j+2)|}{3}, & u - i > 0.5. \end{cases}$$

Normalized to g_1, g_2, g_3, g_4, the formula is as follows:

$$t_k = \frac{g_k}{g_1 + g_2 + g_3 + g_4}, \quad k = 1, 2, 3, 4. \tag{7}$$

The method to determine the fusion coefficient is as follows:

$$\psi_k = e^{-\lambda d_k} \times e^{-(1-\lambda)t_k}, \quad (k = 1, 2, 3, 4), \tag{8}$$

where λ is a constant, $0 < \lambda < 1$, used to adjust the interpolation distance and the weight value of the grayscale gradient in the fusion coefficient.

The formula for normalizing Ψ_k is as follows:

$$\omega_k = \frac{\psi_k}{\psi_1 + \psi_2 + \psi_3 + \psi_4}, \quad (k = 1, 2, 3, 4). \tag{9}$$

After data fusion, the grayscale value of the point P to be interpolated is as follows:

$$y = \omega_1 y_1 + \omega_2 y_2 + \omega_3 y_3 + \omega_4 y_4. \tag{10}$$

At this point, the interpolation of point P is completed.

2.2. Solder Paste Area Detection. The PCB images used for inspection are taken with a monochrome industrial camera under red light irradiation and blue light irradiation, referred to as red monochrome images and blue monochrome images, respectively. The images taken under both color light irradiation are of the same size and correspond to the same area on the PCB. They are used to enhance the accuracy, efficiency, and robustness of the detection.

Let the original image f be a grayscale image with N rows and M columns, and the grayscale value of the pixel at the coordinates (x, y) is denoted as $f(x, y)$. The average grayscale value T_{ave} of the whole image is calculated by the following formula:

$$T_{\text{ave}} = \frac{1}{\text{MN}} \sum_{y=1}^{N} \sum_{x=1}^{M} f(x, y). \tag{11}$$

Calculate the average grayscale value T_{ave1} between T_{ave} and 255.

$$T_{\text{ave1}} = \frac{1}{\text{num}} \sum_{(x,y) \in S} f(x, y), \tag{12}$$

where num is the total number of pixels in the image with grayscale values between T_{ave} and 255 and S is the set of pixels with grayscale values between T_{ave} and 255.

A Gaussian model is created for the red monochrome image and blue monochrome image with pixel grayscale values in the interval T_{ave1} to 255, respectively, its grayscale mean value μ and standard deviation σ are found, and the binarization model is set as follows:

$$g(x, y) = \begin{cases} 255, & \text{if } \mu - 3\sigma < f(x, y) < \mu + 3\sigma, \\ 0, & \text{otherwise.} \end{cases} \tag{13}$$

Binarize the red monochrome images and the blue monochrome images according to the model shown in (14), respectively, and then according to formula (15) for the binary AND operation to obtain the binarized result image.

$$g_o(x, y) = \begin{cases} 255, & \text{if } g_r(x, y) = 255 \text{ and } g_b(x, y) = 255, \\ 0, & \text{otherwise,} \end{cases} \tag{14}$$

where $g_r(x, y)$ and $g_b(x, y)$ are the grayscale values of the pixel at (x, y) in the binarized red and blue monochrome images, respectively. $g_o(x, y)$ is the grayscale value of the pixel at (x, y) in the resulting image. When grayscale values of pixels are 0, they are background pixels and will not be processed. If grayscale values of pixels are 255, the pixels are target pixels. The solder paste areas are obtained.

2.3. Connected Domain Labeling. The labeling of solder paste regions is a prerequisite for printing defect inspection of solder pastes. An improved method is proposed here to reduce the high time complexity in existing connected domain labeling algorithms.

For a target pixel, the grayscale values of pixels in a specific neighborhood are detected according to the location of the target pixel, and the label is set according to specific rules. All the different location types of pixels in the binary image are shown in Figure 2.

Set a two-dimensional array label$[y][x]$, which is used to store the label of the pixel at the location of (x, y) coordinates in the image, and set a one-dimensional array belong[label$[y][x]$], which is used to store the label of the connected domain to which the pixel at the location of (x, y) coordinates belongs, and set the coordinates of the current pixel as (x, y), in the following three cases:

(1) If the current pixel and its neighboring pixels both have different grayscale values, then label$[y][x]$ is the maximum value of the existing initial concatenated domain label plus 1 and set belong[label$[y][x]$] = label$[y][x]$

(2) If the current pixel has the same grayscale value as only one of its neighboring pixels, let the coordinates of the pixel with the same grayscale be (i, j) and then label$[y][x]$ = label$[j][i]$

(3) If the current pixel has m ($m \geq 2$) identical grayscale values with its neighboring pixels, take the pixel with the smallest initial connected domain label value among these m identical grayscale pixels, and note its coordinates as (i, j), then label$[y][x]$ = label$[j][i]$

At this point, after a complete scan of the image, the initially connected domain label and the belonging connected domain label are marked

Then, set a one-dimensional array temp$[T]$, where T is greater than or equal to the maximum of belong [label$[y][x]$], set a variable var, and initialize it to 1

The initial concatenated domain labeled two-dimensional array label$[y][x]$ is scanned in the following two cases:

0	1	1	1	1	1
2	3	3	3	3	4
2	3	3	3	3	4
2	3	3	3	3	4
2	3	3	3	3	4
2	3	3	3	3	4

Figure 2: Schematic diagram of different location types of pixels in binary images.

(1) If label[y][x] = 0, the pixel at coordinates (x, y) is a background pixel and is not processed

(2) If label[y][x] ≠ 0, the pixel at coordinates (x, y) is the target pixel in the following two cases:

(1) If temp[belong[label[y][x]]] = 0, the connected domain label appears for the first time, set temp[belong[label[y][x]]] = var, label[y][x] = temp[belong[label[y][x]]], var = var + 1

(2) If temp[belong[label[y][x]]]≠0, then the label of the connected domain has already appeared, set label[y][x] = temp[belong[label[y][x]]]

The label[y][x] stores the final label of the connected domain in the area where the pixel is located at coordinates (x, y).

2.4. Defects Detection and Types Classification. The types of defects studied here are Excessive Solder, Insufficient Solder, Solder Offset, Solder Bridge, Missing Printing, and Spattering Solder, as shown in Figure 3. The paper studies the characteristics of different defects and compares the connected domains between the labeled result image and standard image to propose the inspection rules to find the defects and identify their types.

Calculate the area and centroid of the solder paste area A with the following equation:

$$S = \sum_{(x,y)\in A} 1, x_0 = \frac{1}{N}\sum_{(x,y)\in A} x, y_0 = \frac{1}{N}\sum_{(x,y)\in A} y, \tag{15}$$

where (x, y) are the coordinates of the pixels in the solder area, S is the area of the solder area, N is the total number of pixels in the solder area, and (x_0, y_0) is the centroid of the solder area. The connected domain with an area less than a certain threshold T_0 is treated as noise and is not used for defect inspection.

Step 1. By means of the centroid coordinates, find the label of the corresponding connected domain in the standard image of all the solder-paste connected domains in the resulting image.

If the label is 0, it corresponds to the background area and is not processed. If the label is not 0, the following two cases can be distinguished:

(1) If there are duplicate labels, it means that Solder Bridge has occurred.

(2) For a nonrepeat label, it indicates that Solder Bridge has not occurred and continues with other defect type inspections.

T_1 and T_2 are preset thresholds, $T_1 < 1$, $T_2 > 1$. Take one out of all the nonrepeated labels, suppose its connected component area is S_f, and the corresponding connected component area in the standard image is S_b.

(1) If $S_f/S_b < T_1$, the connected domain is determined to be Insufficient Solder.

(2) If $S_f/S_b > T_2$, the connected domain is determined to be Excessive Solder.

(3) If $T_1 \le S_f/S_b \le T_2$, then it means there are no Excessive Solder and Insufficient Solder and continues to Solder Offset inspection.

Assuming that the centroid coordinates of the connected domain in the standard image are (x_b, y_b), the centroid coordinates of the corresponding connected domain in the resultant image are (x_f, y_f), T_3 is a predetermined threshold, and the centroid position deviation d is expressed as follows:

$$d = \sqrt{\left(x_b - x_f\right)^2 + \left(y_b - y_f\right)^2}. \tag{16}$$

① If $d \le T_3$, the connected domains are judged to be normal.

② If $d > T_3$, the connected domains are judged as Solder Offset.

Step 2. Through centroid coordinates, find out the connected domain labels in the standard image corresponding to all the unprocessed solder paste connected domains in the resulting image, and record all the labels:

(1) If the label is 0, the connected area of solder paste is judged as Spattering Solder.

(2) If there is a nonzero repeated label in the label record, it means that multiple solder paste connected domains in the resulting image correspond to one solder paste connected domain in the standard image, and data merging is required. After data merging, the operation is similar to Step 1.

(3) For nonzero and nonrepetitive labels, there is no need to merge data. The operation is exactly the same as the processing of nonrepetitive labels in Step 1.

Step 3. After the processing of the above steps, if there are unprocessed connected domains, it indicates that a Missing Printing has occurred.

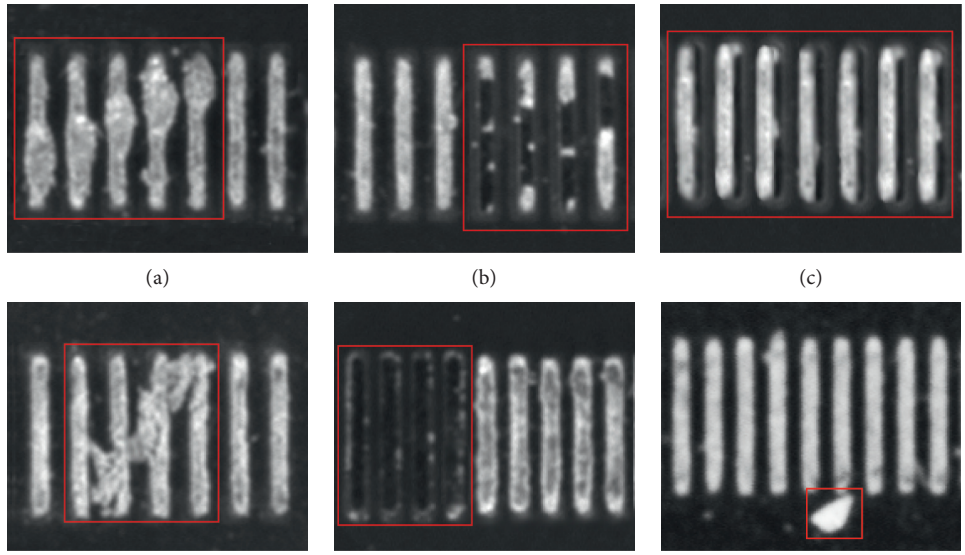

Figure 3: Six types of defects: (a) Excessive Solder, (b) Insufficient Solder, (c) Solder Offset, (d) Solder Bridge, (e) Missing Printing, and (f) Spattering Solder.

3. Results and Discussion

3.1. Image Interpolation Experiment. The original image is shown in Figure 4(a), which is sampled three times to reduce its length and width to 50%, 70%, and 30% of the original one, respectively. Then, the bilinear, bicubic, and the proposed methods in this paper are interpolated, respectively, and due to space limitation, only 30% of the resulting images are given as shown in Figures 4(b), 4(c), and 4(d).

Calculate the peak signal-to-noise ratio with the following equation:

$$\mathrm{PSNR} = 10\log_{10}\frac{255^2}{(1/\mathrm{MN})\sum_{x=1}^{M}\sum_{y=1}^{N}\left(f(m,n)-\widehat{f}(m,n)\right)^2}, \tag{17}$$

where M and N are the horizontal and vertical sampling points of the image, respectively, $f(m, n)$ is the original image, and $\widehat{f}(m, n)$ is the processed image. The larger the PSNR value, the higher the accuracy of the interpolation algorithm. Due to space limitations, only the experimental results are given when the image aspect is reduced to 30%, as shown in Table 1. From the table, we can see that the algorithm in this paper has the highest PSNR, indicating that the algorithm has high interpolation accuracy.

3.2. Solder Paste Area Detection Experiment. Three sets of red and blue monochrome images were taken under normal, strong, and weak illumination, respectively, and the binarization method proposed in this paper was used to detect the solder paste area. Here, the detection and result images under weak illumination are given as an example which are shown in Figure 5, where Figures 5(a) and 5(b) are the red and blue monochrome images to be detected, respectively, and Figure 5(c) is the detection result image.

Ten types of solder paste areas were used for detection, as shown in Table 2; due to space limitations, only the results of solder paste detection under weak illumination are given.

The error rate for each type of solder paste area detection is calculated according to the following formula:

$$\mathrm{ER} = \frac{\sum_{i=1}^{N}\left|n_i - n_{io}\right|}{\sum_{i=1}^{N} n_{io}}, \tag{18}$$

where N denotes the number of solder areas of the type, n_i denotes the number of pixels detected in the ith solder area of the type, and n_{io} denotes the true number of pixels in the ith solder area of the type. The smaller the ER, the higher the detection accuracy. From the table, it can be seen that the adaptive threshold binarization method proposed in this paper has a low ER and can achieve high accuracy detection of solder paste areas.

3.3. Connected Domain Labeling Experiment. Six images were labeled with connected domains using the algorithm of this paper, the region growth method [14], and the tour-based coding method [15], respectively. They were executed 10 times consecutively, and the average time was recorded as shown in Table 3. As can be seen from the table, compared with the other two algorithms, the algorithm of this paper has the advantage of a shorter running time.

One of the six images is shown in Figure 6(a). The image labeled using the improved algorithm in this paper is shown in Figure 6(b). Each connected domain in the resulting image is assigned a different grayscale value to show the distinction in labeling.

3.4. Defects Detection and Types Classification Experiment. Figure 7(a) shows the image to be inspected, and Figure 7(b) shows the standard image obtained by parsing

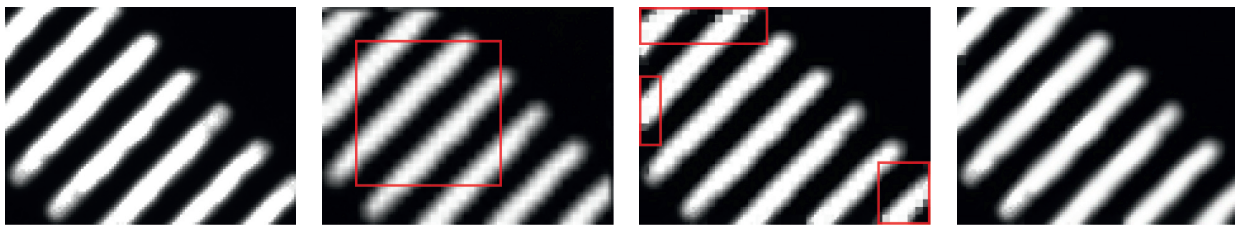

(a) (b) (c) (d)

Figure 4: Interpolated image of the result of reducing the length and width to 30%. (a) Original image. (b) Bilinear interpolation. (c) Bicubic interpolation. (d) Method proposed in this paper.

Table 1: PSNR of interpolation results for each algorithm (unit: decibels).

Algorithm	Image 1	Image 2	Image 3	Image 4	Image 5
Bilinear	24.046	26.524	24.662	22.264	33.798
Bicubic	26.621	27.973	26.733	22.313	36.131
This paper	27.328	28.324	26.998	23.103	37.323

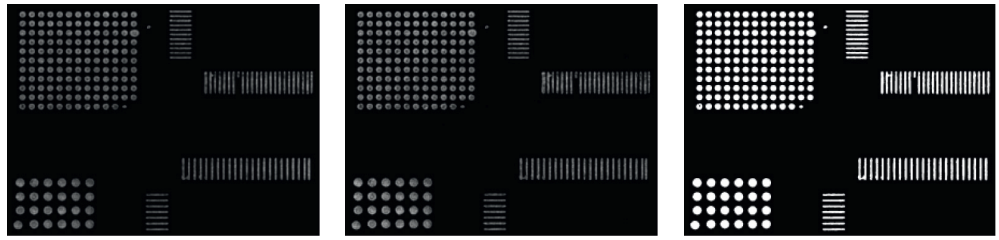

(a) (b) (c)

Figure 5: Original and test resulting images under weak illumination conditions. (a) Red monochrome image. (b) Blue monochrome image. (c) The resulting image.

Table 2: The results of solder paste detection under weak illumination.

Type	Number of connected domains	Pixel-number per connected domain	Average error of pixel-number	ER (%)
Round 1	1	1790	4	0. 2
Round 2	66	1128	4	0. 3
Round 3	55	614	4	0. 6
Round 4	96	254	3	1. 2
Rectangle 1	16	1880	12	0. 6
Rectangle 2	20	832	12	1. 4
Rectangle 3	87	1067	12	1. 1
Rectangle 4	2	679	8	1. 2
Square 1	40	256	8	3. 1
Square 2	120	144	4	2. 7

Table 3: Running times for each image under different algorithms (unit: second).

Algorithm	Image 1	Image 2	Image 3	Image 4	Image 5	Image 6
Reference [14]	0.059	0.338	0.161	0.147	0.168	0.166
Reference [15]	0.262	0.509	0.227	0.221	0.315	0.321
This paper	0.031	0.106	0.042	0.041	0.063	0.063

the Gerber file. The inspection results are shown in Figure 7(c), and the meanings of each letter are as follows: D for Excessive Solder, S for Insufficient Solder, P for Solder Offset, Q for Solder Bridge, L for Missing Printing, and J for Spattering Solder.

Using the results of manual visual inspection as the standard, the inspection accuracy, classification accuracy, and false alarm rate of the defect inspection method studied in this paper were calculated, and the results are shown in Table 4. As can be seen from the table, the

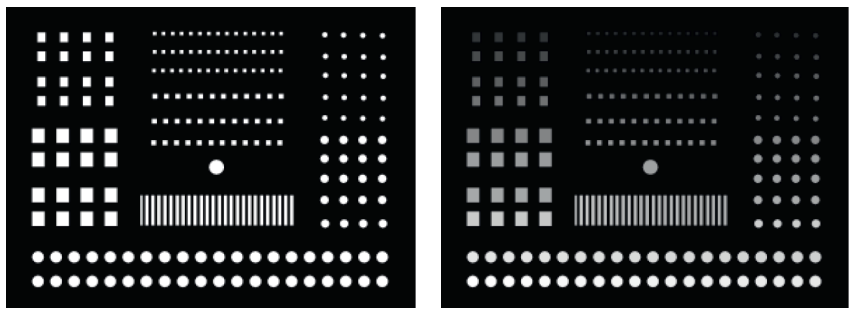

(a) (b)

Figure 6: The experiment of the improved algorithm of this paper. (a) The experiment image. (b) The labeled image.

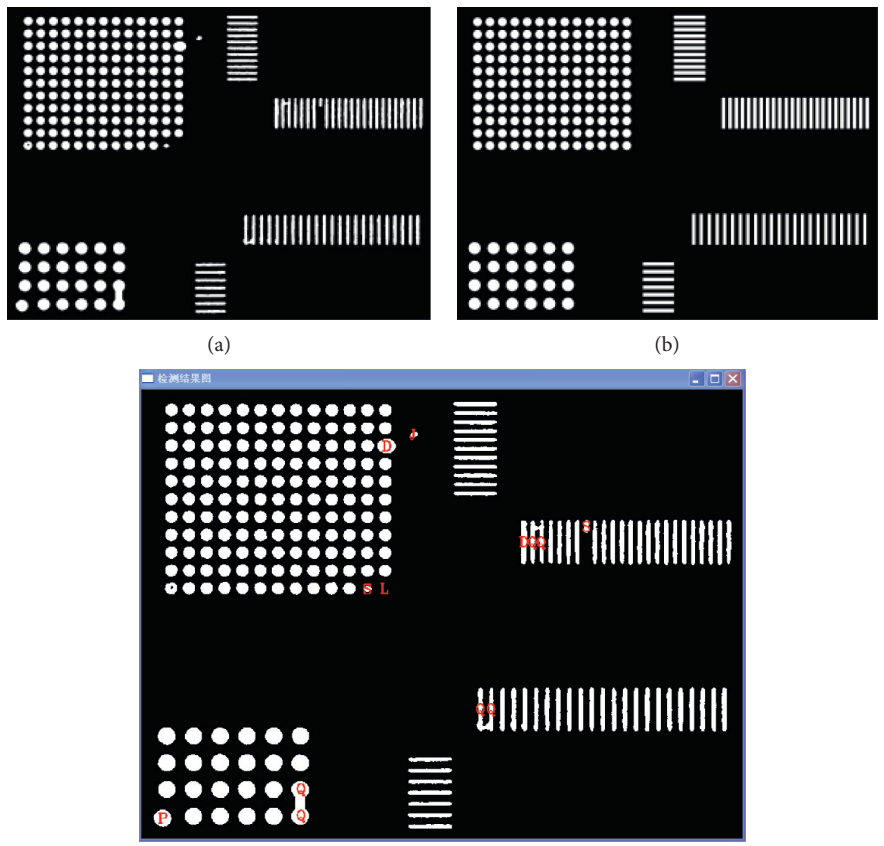

(a) (b)

(c)

Figure 7: (a) Solder paste image to be inspected. (b) Standard image. (c) Inspection result.

Table 4: The inspection results for different types of defects.

Type of defect	Excessive Solder (%)	Insufficient Solder (%)	Solder Offset (%)	Solder Bridge	Missing Printing (%)	Spattering Solder	Average (%)
Inspection accuracy	100	100	100	99.17%	100	100%	99.86
Classification accuracy	100	96.77	100	96.67%	97.78	100%	98.54
False alarm rate	0.03	0.04	0.05	0	0.02	0	0.14

proposed method can inspect six types of defects with a high inspection and classification accuracy and low false alarm rate.

4. Conclusion

In this paper, the techniques related to the inspection of solder paste images and printing defects are studied and some substantial results are achieved. The proposed regional multidirectional data fusion image interpolation method not only has a fast interpolation speed but also has a high interpolation accuracy, can protect the edge details of the image well, and is applicable to any level of interpolation transformation, and the interpolation method is applied to PCB image registration, which improves the speed and accuracy of registration. The proposed solder paste region detection scheme can accurately identify solder paste regions and can adapt well to changes in light source brightness with low time complexity. The proposed solder paste printing defect inspection method is able to detect six types of defects with low time consumption and has good performances in inspection and classification. However, the research work in this paper is aimed at external defects inspection and cannot deal with internal cavity defects detection. Moreover, the method is studied for the inspection work in two-dimensional space, which cannot detect those defects when needing height or depth information, for example, scars inspection, pits inspection, and so on. Three-dimensional defect inspection is worth studying, where highly accurate height or depth detection is the key technology.

Data Availability

The datasets used and/or analyzed during the current study are available from the corresponding author on reasonable request.

Conflicts of Interest

The authors declare no conflicts of interest.

Acknowledgments

The authors acknowledge the funding of the Key Project of Shaanxi Province Innovation Program, China (2017ZDCXL-GY-11-02-02).

References

[1] P. Huang, C. S. Guo, H. H. Chen, and H. K. Zhang, "A survey of image registration methods based on deep learning," *Journal of Hangzhou Dianzi University (Natural Sciences)*, vol. 40, no. 06, pp. 37–44, 2020.

[2] J. S. Zhang, H. M. Zhang, Y. T. Luo, and B. Y. Chen, "Lmage registration method based on improved Harris corner detection algorithm," *Laser & Infrared*, vol. 47, no. 02, pp. 230–233, 2017.

[3] G. S. Ding, Y. L. Qiao, W. N. Yi, L. L. Du, and W. Fang, "Lmproved SIFT feature extraction and matching technology based on hyperspectral image," *Optics and Precision Engineering*, vol. 28, no. 04, pp. 954–962, 2020.

[4] C. Y. He, Z. W. Zheng, and Y. Lu, "Mobile terminal dynamic background moving target detection based on SURF and FREAK," *Journal of Optoelectronics - Laser*, vol. 30, no. 02, pp. 146–153, 2019.

[5] F. Q. Zhao, "Image registration method based on gray information," *Computer & Digital Engineering*, vol. 47, no. 10, pp. 2568–2572, 2019.

[6] J. Zheng, W. Song, Y. Wu, and F. Liu, "Image interpolation with adaptive k -nearest neighbours search and random nonlinear regression," *IET Image Processing*, vol. 14, no. 8, pp. 1539–1548, 2020.

[7] P. B. Fu, H. J. Tie, and H. R. Yang, "Image interpolation algorithm based on texture details and edge structure maintained," *Application Research of Computers*, vol. 38, no. 04, pp. 1203–1207 + 1211, 2021.

[8] H. Y. Qian, "A medical image edge detection algorithm based on improved Canny operator," *Software Guide*, vol. 18, no. 02, pp. 45–48, 2019.

[9] B. A. Hussain and M. S. Hathal, "Development of Iraqi license plate recognition system based on Canny edge detection method," *Journal of Engineering*, vol. 26, no. 7, pp. 115–126, 2020.

[10] R.-G. Zhou, H. Yu, Y. Cheng, and F. X. Li, "Quantum image edge extraction based on improved Prewitt operator," *Quantum Information Processing*, vol. 18, no. 9, pp. 1–24, 2019.

[11] Y. Liu and C. L. Xia, "An image edge detection algorithm for strip steel surface defects based on Sobel operator," *Electronic Measurement Technology*, vol. 44, no. 03, pp. 138–143, 2021.

[12] Z. Zhang, "Research and analysis of 3D SPI based on measuring profilometry," *Equipment for Electronic Products Manufacturing*, vol. 47, no. 05, pp. 37–44, 2018.

[13] W. H. Wang and P. X. Li, "Research on defect detection system of SMT chip based on machine vision," *Wireless Internet Technology*, vol. 12, pp. 99-100, 2017.

[14] Z. Luo, Y. Zhou, and Z. Zheng, "Optimization of connected domain labeling algorithm based on region growth," *Journal of Minjiang University*, vol. 32, no. 2, pp. 41–44, 2011.

[15] Q. Liu and X. Gong, "A new method for labeling connected regions of binary images," *Computer Engineering and Applications*, vol. 48, no. 11, pp. 178–180, 2012.